Mechanism underlying the ultralow energy-consumption rapid ion dehydration for the high flux of KcsA potassium channels

Yue Wang[1], Bo Song[2,*], Lei Jiang[3,4,5,*]

[1]Hubei Key Laboratory of Agricultural Bioinformatics, College of Informatics, Huazhong Agricultural University, Wuhan 430070, China.

[2]School of Optical-Electrical Computer Engineering, University of Shanghai for Science and Technology, Shanghai 200093, China.

[3]State Key Laboratory of Bioinspired Interfacial Materials Science, Suzhou Institute for Advanced Research, University of Science and Technology of China, Suzhou, Jiangsu 215123, China.

[4]Nano Science and Technology Institute, University of Science and Technology of China, Hefei 230026, China.

[5]Institute for Biomedical Materials & Devices (IBMD), Faculty of Science, University of Technology Sydney, Sydney, NSW 2007, Australia.

*Corresponding author email: bsong@usst.edu.cn, jianglei@iccas.ac.cn

High-flux and ultralow energy consumption transport of biological and artificial ion channels has been widely reported [1-22]. However, there is a precondition for such transport: Ultralow energy-consumption rapid ion dehydration; its mechanism is a remaining challenge. Here, we demonstrate that a K^+ ion can transfer from the hydration water outside KcsA channel to the water bound in the channel without its hydration water accompanying, i.e., a tunneling-like motion, which provides a basis for the ultralow energy-consumption ion dehydration. In our molecular dynamics simulations, a KcsA channel was divided into three regions: Cavity-1, Cavity-2 and filter. As a hydrated K^+ ion moves from Cavity-1 to Cavity-2, there occurs a resonant energy transfer to the ion from the filter-confined coherently oscillating ions,

leading to a tunneling-like motion of the ion from the Cavity-1 water to Cavity-2 water with no hydration shell accompanying and no influence on the Cavity-2 water. As the hydrated K^+ ion further moves from Cavity-2 to KcsA filter, the ion adjusts its hydration-shell water structure to coherence-resonantly couples with the filter-confined ions, leading to another tunneling-like ion motion to reach complete dehydration. Such two processes cause directionally rapid ion dehydration of KcsA channel, as a basis for the high flux of channel. Our findings provide an understanding of the dehydration dynamics in biological channels and its relationship with the high flux of ultralow energy-consumption, potentially promoting the development of artificial membranes design.

Key words: resonance; tunneling-like ion dehydration; high flux; biological channels

The high flux as well as the high selectivity is the character of biological ion channels, enabling the ultralow energy consumption and ultrahigh accuracy of biological systems **[1]**. Inspired by the biological channels, a large amount of artificial membranes with nanopores are designed to achieve ion transport with a high flux (~10^8 ions·s^{-1}) as well as high selectivity **[2-21]**. These advances in turn urgently call for the understanding of biological channels. Mackinnon and colleagues deeply studied ion selectivity of potassium channels a quarter century ago, and attributed it to the special structure of the ion-selective filter **[22]**. de Groot et al. proposed a direct Coulomb knock-on model for K^+ ions permeating the channel, i.e., the Coulomb repulsion between adjacent ions is a key to the high-efficiency ion conduction **[23]**. Zanni et al. suggested a knock-on model in which K^+ ions and water molecules exhibit alternate passage through the filter **[24]**. The further investigation of de Groot et al. showed that the completely-dehydrated K^+ ions occupy all the filter sites in the transport process, i.e., a direct knock-on model **[25]**. Recently, we demonstrated a quantum coherence model for the high-ordered ion transport, i.e., the filter-confined K^+ ions move together as a coherent body, which determines the high flux and ultralow energy consumption of KcsA channel **[26]**. Despite these, there is a remaining issue: As a precondition for the high-flux and ultralow energy consumption transport of channels, a hydrated ion should conduct rapid and ultralow energy consumption dehydration before it transports in the channel.

To realize the ultralow energy consumption dehydration of ion channel, we believe that there needs a condition, i.e., the hydration water of an ion does not accompany the ion into the channel; otherwise the water back-flow will cause huge energy consumption. Therefore, during the process, the number of water molecules bound in the channel will remain unchanged. Applying the KcsA potassium channel as a typical example, we show this hypothesis detailedly. There are a hydrophilic gate and a hydrophobic gate in the channel (**Fig. 1a**). The channel is thus divided into three regions: the cavity outside of the hydrophilic gate, the cavity between the hydrophilic and hydrophobic gates,

and the Fitler+ inside of the hydrophobic gate. A hydrated K^+ ion initially outside the channel moves toward the channel, and has no interaction with the channel-confined ions (**Fig. 1a left**). As the ion moves close to the hydrophobic gate, an interaction with the channel-confined ions may form, causing that the hydrated ion passes through the hydrophilic gate (**Fig. 1a middle**). In the process, the hydrated ion undresses its hydration shell and then redresses a new one in the cavity between two gates, i.e., a tunneling-like ion motion passing through the hydrophilic gate without its hydration water accompanying. After that, the ion continues to pass through the hydrophobic gate and move into Filter+ (**Fig. 1a right**), while the ion undresses its hydration shell and achieves the complete dehydration. Therefore, no shell water accompanies the K^+ ion in the whole process of moving in the channel, and then the effect of ion dehydration on the bound water in the cavity outside of hydrophilic gate and the cavity between hydrophilic and hydrophobic gates should be ignorable.

To examine this hypothesis, using molecular dynamics (MD) simulations on a KcsA channel system, we demonstrate that a K^+ ion can transfer from the hydration water outside the channel to the water bound in the channel without its hydration water accompanying, i.e., a tunneling-like motion, which provides a basis for the ultralow energy-consumption ion dehydration (**Fig. 1b,c**). During the process, water in the channel remains unchanged. Specifically, as a hydrated K^+ ion moves from Cavity-1 to Cavity-2, there occurs a resonant energy transfer to the ion from the filter-confined coherently oscillating ions, causing a tunneling-like motion of the ion from the Cavity-1 to Cavity-2 water with no hydration shell accompanying and no influence on the Cavity-2 water. As the hydrated K^+ ion further moves from Cavity-2 to KcsA filter, the ion adjusts its hydration-shell water structure to coherence-resonantly couples with the filter-confined ions, leading to another tunneling-like ion motion to reach complete dehydration. Such two processes cause directionally rapid ion dehydration, providing a basis for the channel high-flux of ultralow energy-consumption.

Results and Discussion

To explore the dehydration process of a K^+ ion when it passes through a potassium channel, we performed MD simulations on a KcsA channel system. The transmembrane voltage (*V*) of a neural K^+ current is usually in the range of ~80 mV **[27]**. An open KcsA channel system under *V* = 100 mV was thus applied (**Fig. 1c left**, **Supplementary Fig. 1**). There were seven sites of ion occupation in the channel, labeled S01, S02, S1, S2, S3, S4 and S03 (**Fig. 1c right**). A hydrophilic residue-formed gate was located between S01 and S02, and a hydrophobic residue-formed gate was between S02 and S1, labeled hydrophilic and hydrophobic gates, respectively. We thus divided the channel into three regions: Cavity-1, Cavity-2 and Filter+. The density distribution of water was calculated. As shown in **Fig. 1d left**, the density of water in the KcsA entrance terminal was 32.2 ± 0.3 nm^{-3}, consistent with that (~32 nm^{-3}) of bulk water. A clear region of density minima between Cavity-1 and Cavity-2 was observed, due to the influence of the hydrophilic gate. In Cavity-2, there was a density maximum, related to the hydrophilic effect of Cavity-2 on-wall threonine (Thr) residues at *Z* ~ -7.1 Å. From the Thr residues to filter, the density decreased, due to the influence of the hydrophobic gate. To study the effects of the above two gates on the ion shell water, we calculated the hydration number when the ion transports through the channel. The H_2O number of 1st-shell water kept on a plateau of 6.4 ± 0.1 both in Cavity-1 and Cavity-2, and that of 2nd-shell water decreased from 20.2 to 17.2 in Cavity-1 and decreased to 9.5 from a plateau of 17.2 ± 0.2 in Cavity-2 (**Fig. 1d right**). The fluctuation of 2nd-shell H_2O number was clearly limited when the ion was at the hydrophilic gate, meaning a clear effect of the gate on the hydration shell. In-between the hydrophobic gate and filter, the H_2O numbers of ionic 1st and 2nd hydration shells decreased to 0.8 and vanishing, respectively, denoting complete dehydration. Although the radial distributions of 1st-shell water in Cavity-1 and Cavity-2 were very similar, those of 2nd-shell water were different, with maxima at 4.5 Å and 5.0 Å, respectively (**Fig. 1e**). Therefore, water in Cavity-2 is clearly different from that in the other regions, while the significant changes in K^+ ion hydration shells occur when the ion moves from Cavity-1 to Cavity-2

(labeled Proc-I) and from Cavity-2 to filter (labeled Proc-II), with the great effects of the hydrophilic and hydrophobic gates, respectively.

Resonant energy transfer-driven tunneling-like dehydration when a hydrated K^+ ion moves from the KcsA Cavity-1 to Cavity-2 (i.e., Proc-I). To study the dehydration in Proc-I, we analyzed the structure change of water in Cavity-2 as a hydrated ion enters. The typical trajectories of hydrated ion *Z*-coordinate and Cavity-2 H_2O number are shown in **Fig. 2a left**. For the time *t* = 350 ps to 380 ps, the hydrated ion K0 moved from *Z* = -14.3 Å to -8.5 Å, passing through the hydrophilic gate to Cavity-2. During the process, the number of H_2O in Cavity-2 weakly fluctuated in the range of 33 to 40 with an average of 36.5 ± 1.5, indicating that the change of Cavity-2 water is slight. The distribution of Cavity-2 H_2O had a significant maximum at *Z* = -7.1 Å (the location of hydrophilic Thr), denoting that the Thr residues on the Cavity-2 wall have an attraction to the H_2O molecules. Over all our simulations the distributions of Cavity-2 H_2O number in the absence and presence of K^+ ion well matched each other, with an identical average value of 39 ± 3, meaning that the Cavity-2 H_2O number is independent of the ion (**Fig. 2a right upper**). The previous error (±1.5) of Cavity-2 H_2O number (36.5 ± 1.5) caused by K0 entering was in the range here (±3) of spontaneous Cavity-2 water fluctuation, indicating that the effect of K^+ ion entry on Cavity-2 water is ignorable. All these analyses suggest that the hydration water accompanying the ion into Cavity-2 can be ignored, and the 39 ± 3 H_2O molecules are well confined in Cavity-2 with help of hydrophilic Thr residues on the cavity wall. The property of Cavity-2 confined water over all the simulations was further studied. The number density of Cavity-2 water was 21.7 ± 1.7 nm^{-3} and 21.6 ± 1.7 nm^{-3} in the absence and presence of K^+ ion, respectively, while that of bulk water was 32.15 ± 0.01 nm^{-3} (**Fig. 2a right lower**). The ion-caused slight change of only 0.5% in the Cavity-2 confined water density also supports that the shell water accompanying the ion into Cavity-2 is ignorable. The density of Cavity-2 water was significantly smaller than that of bulk water, and the fluctuation was much larger than that of bulk water. The water

confined in Cavity-2 is thus in a state between liquid and gas, different from the incompressible liquid water, providing a feasibility for the tunneling-like motion of a naked ion from the Cavity-1 water to Cavity-2 water, different from the conventional diffusion of hydrated ions. Hence, we can conclude that the ion of a hydrated ion passes through the hydrophilic gate into Cavity-2 without the hydration shell accompanying (i.e., tunneling-like dehydration), and the ion-caused change in the Cavity-2 confined water is ignorable.

To explore the driving force for a hydrated K^+ ion to replace its hydration shell in the tunneling-like dehydration process, we analyzed dynamics spectra of KcsA ion transport. When a hydrated ion (K0) moved from the outside towards the filter, three ions (K1, K2, K3) were confined in the filter and performed coherent oscillation (**Fig. 2b left**) **[26]**. At the time $t = t_0$, t_1, t_2, t_3 and t_4, K0 was successively outside the channel, in Cavity-1, at the hydrophilic gate, in Cavity-2, and in Filter+ (but outside the filter). Spectra of the filter-confined ion oscillation and hydrophilic gate vibration at the time t_i, (i = 0, 1, 2, 3, 4) were calculated, respectively **[26]**. As shown in **Fig. 2b middle**, at $t = t_0$, there were three vibration peaks of the hydrophilic gate at 40.5 THz, 42.4 THz and 44.6 THz, three oscillation peaks of the filter-confined ions at 39.4 THz, 40.2 THz and 40.6 THz, respectively. For $t = t_1$ (K0 in Cavity-1), the changes in locations and intensities of the hydrophilic gate peaks clearly occurred, indicating that the K0 starts to couple with the gate, affecting the gate vibration. The peaks of filter-confined ions kept their initial states, denoting that the effect of K0 on K1, K2 and K3 is ignorable. At $t = t_2$ (K0 at the hydrophilic gate), instead of the previous three peaks of hydrophilic gate, two huge peaks were observed at 39.4 THz and 41.0 THz, respectively, which means that the full coupling of K^+ ion with the gate is achieved, resulting in a new vibration structure. As for the filter-confined ions, the 39.4-THz and 40.6-THz peaks disappeared, and the 40.2-THz peak intensity clearly decreased, denoting that the K0 at the hydrophilic gate has a significant long-range effect on the confined ions in the filter, causing a great energy loss of them. Remarkably, the disappearing 39.4-THz peak had an identical

frequency to the first peak of ion-coupled gate, and the disappearing 40.6-THz peak well matched the second one (41.0 THz) in the frequency. These facts mean that two resonant channels between the filter-confined ions and hydrophilic gate occur at the time t_2, and the oscillation energy of confined ions is resonantly transferred to the ion-coupled gate (**Fig. 2b right**). Huge peaks of the ion-coupled gate indicate huge amplitudes of the gate and hydrated ion vibration, providing a force for the ion to overcome its coupling with the shell water, as is followed by the ion redressing a new hydration shell in Cavity-2. During $t = t_3$ to t_4, both the spectra of hydrophilic gate and filter-confined ions recovered to their initial cases, meaning that the K0 effect disappears as K0 leaves. Therefore, when a K^+ ion passes through the KcsA hydrophilic gate, there is resonant energy transfer from the filter-confined coherently-oscillating ions to the ion-coupled gate, which drives the ion to replace its hydration shell by a new one to achieve the tunneling-like dehydration.

Note: the blackbody radiation of surroundings at body temperature is located at the wavelength of ~9 μm with the full width at half maximum of 11 μm, i.e., at the frequency of ~34 THz, well covering the filter-confined ion coherence oscillation of ~40 THz (**Fig. 2b middle right bottom**) **[28]**. In principle, after the ion leaves the hydrophilic gate, the spontaneous radiation of surroundings will supplement the resonantly-transferred energy of filter-confined ions with a high efficiency.

Coherent resonance-caused tunneling-like dehydration when a hydrated K^+ ion moves from the KcsA Cavity-2 to filter (i.e., Proc-II). To study the dehydration in Proc-II, we analyzed the trajectories of ions and hydration number during a hydrated ion moves from Cavity-2 to the filter. Typical trajectories of the ion *Z*-coordinates (K0, K1, K2, K3) and the K0 1st-shell H_2O number are shown in **Fig. 3 top and middle**. Overall, in the time of t = 431.3 ns to 437.8 ns, as K0 oscillated and moved to the filter, its 1st-shell H_2O number oscillated and decreased, indicating multiple adjustments of the hydration shell as the K0 moves. K1, K2 and K3 were confined in the sites S2, S3 and S4 of filter, respectively, with ignorable fluctuations in the trajectories from 431.3 ns to 432.05

ns and obvious ones from 432.05 ns to 437.8 ns, i.e., K0 has an influence on filter-confined ions only as it is close to the hydrophobic gate. Specifically, in the time t = 431.3 ns to 432.05 ns, the K0 moved towards the hydrophobic gate, and its 1st-shell H_2O number was on a plateau of 6.5 ± 0.4. For t = 432.05 ns to 435.8 ns, as the K0 oscillated and passed through the hydrophobic gate to site S1, the 1st-shell H_2O number oscillated and declined from 6.3 to a plateau of 1.6 ± 0.1, meaning multiple adjustments of the hydration shell near this gate. In a short time from 435.8 ns to 436.1 ns (labeled the time region I), with K0 moving rapidly moving back to the hydrophobic gate, the shell water number significantly increased from 1.7 to 4.5, meaning a large adjustment of the hydration shell. For t = 436.1 ns to 437.8 ns, as K0 migrated from a plateau of Z = -2.2 ± 0.2 Å (close to the hydrophobic gate) to a plateau of Z = -0.4 ± 0.2 Å (close to the site S1), its shell H_2O number decreased from plateaus of 4.0 ± 0.2 to 1.6 ± 0.1. After that, in a short time from 437.8 ns to 437.96 ns (labeled the time region II), K0, K1, K2 and K3 synchronously underwent rapid transfer, with K3 exiting the filter and the ions K0, K1, K2 moving to the sites S2, S3, S4, respectively. The K0 ion hydration number declined from 1.7 to 0.5, meaning complete dehydration. The water molecule of accompanying the K0 into the filter thus can be ignored, thereby the process of t = 432.05 ns to 437.96 ns can be regarded as tunneling-like dehydration too. Finally, in 437.96 ns to 439.0 ns, K3 left the channel, the K0, K1, K2 kept at the S2, S3, S4, respectively, and the K0 hydration number on a plateau of 0.5 ± 0.2. Thereby, as the ion hydration shell structure is adjusted, another tunneling-like dehydration occurs when a K^+ ion moves from Cavity-2 to the filter, while the ion has an influence on the filter-confined ions when it is close to the hydrophobic gate, which potentially in turn plays a role in the ion dehydration.

To explore the action of filter-confined ions on the ion of tunneling-like dehydration near the hydrophobic gate, we introduced the coherence degree of the hydrated ion with the filter-confined ions and that of the filter-confined ions. The coherence degrees were defined as,

$$\alpha_{01\ldots N} = \frac{1}{2C_N^2}\sum_{i\neq j}^{N}\frac{\vec{v}_i\cdot\vec{v}_j}{|\vec{v}_i||\vec{v}_j|},$$

where the $\vec{v}_i$ (or $\vec{v}_j$) indicates the velocity of the ith (or j^{th}) K^+ ion, with the ion labels i, j = 0, 1, 2, …, while N denotes the ion number. The coherence degree ($\alpha_{0\text{-}123}$) of the hydrated ion K0 with the filter-confined ions K1, K2 and K3 was calculated by the equation $\alpha_{0\text{-}123} = (\alpha_{01} + \alpha_{02} + \alpha_{03})/3$ with $N = 2$. The coherence degrees of three filter-confined ions, i.e., K1 – K3 (i, j = 1, 2, 3) for the time t = 431.3 ns to 437.96 ns and K0 – K2 (i, j = 0, 1, 2) for t = 437.96 ns to 439.0 ns, were calculated with $N = 3$, respectively, labeled α_{123} and α_{012}.

By the coherence degrees, we analyzed the fine interaction process of a hydrated ion with the filter-confined ions as well as its effect on the tunneling-like dehydration. As shown in **Fig. 3 bottom**, during t = 431.3 ns to 432.05 ns, the coherence degree α_{123} of filter-confined ions K1, K2 and K3 was on a plateau of 0.46 ± 0.02 with a very slight fluctuation, which corresponds to the fluctuation-ignorable ion coordinate trajectories of **gray blue in Fig. 3 middle**. Thus, the K0 effect on the K1, K2 and K3 coherence is very weak when K0 is in Cavity-2, and the three filter-confined ions are in a coherent oscillation state. The coherence degree $\alpha_{0\text{-}123}$ of K0 with K1, K2 and K3 was less than 0.1, denoting that K0 is incoherent with other three ions, corresponding to the plateaus (**Fig. 3 middle, green & orange**) of the hydrated ion. During t = 432.05 ns to 435.8 ns, the coherence degree α_{123} clearly fluctuated in the range of 0.26 to 0.61 with a period (T_{123}) of ~3 ns, different from the above plateau of α_{123}. Namely, as K0 is close to the hydrophobic gate, assisted by the gate, a coupling of K0 with K1, K2 and K3 forms, causing a perturbation on the coherent oscillation of filter-confined ions. The degree $\alpha_{0\text{-}123}$ was in the range of 0.01 to 0.35 with a fluctuation period ($T_{0\text{-}123}$) of ~2 ns, meaning that the coupling of K0 with K1, K2 and K3 causes coherence between them. The difference of fluctuation periods T_{123} and $T_{0\text{-}123}$ denotes that although the coherence occurs, the K0 still does not well coherently match the oscillation of the confined ions, i.e., they are in a coherence-matching process. In this process, to make K0 coherently match the filter-confined ion oscillation, the K0 shell

water structure is multiply adjusted, i.e., the huge fluctuation (**Fig. 3 middle, orange**) of hydration number. In the time region I of 435.8 ns to 436.1 ns, the degrees α_{123} and $\alpha_{0\text{-}123}$ increased from 0.31 to 0.40 and from 0.03 to 0.10, respectively. From 436.1 ns to 437.96 ns, α_{123} kept on a plateau of 0.44 ± 0.03, consistent with their initial plateau of 0.46 ± 0.02, while $\alpha_{0\text{-}123}$ increased from 0.10 to 0.30, and its difference with α_{123} (0.35) at 437.96 ns is small enough to ignore. Namely, by the last adjustment of hydration shell in the time region I, the coherent-resonance coupling of K0 with three filter-confined ions is achieved, causing a coherent body of four ions moving together towards the exit in the time region II (**Fig. 3 middle, green & gray blue**). This process responds to that after the hydration-shell adjustment, the hydration number (**Fig. 3 middle, orange**) of K0 ion decreases from 4.5 to 0.5. From 437.96 ns to 439.0 ns, as K3 left the channel, α_{012} kept on a plateau of 0.45 ± 0.02, consistent with the initial value (0.46 ± 0.02) of α_{123}, meaning that the coherent oscillation of filter-confined ions recovers. Therefore, we can conclude that through adjusting the structure of K^+ ion hydration shell assisted by the hydrophobic gate, the ion forms a coherent resonance with the filter-confined coherently-oscillating ions, causing the tunneling-like dehydration near this gate.

All these results suggest a resonant tunneling of the K^+ ion from the KcsA outside to filter. As shown in **Fig. 4a**, the hydrophilic and hydrophobic gates (labeled Gate-1 and Gate-2) provide two barriers (labeled Barrier-1 and Barrier-2) in the ion transport pathway from the area A (outside of channel) to the areas B (outside of Gate-1), C (between Gate-1 and Gate-2) and D (filter). There are the bound states of ion in the areas B and C, labeled BS-1 and BS-2, respectively (**Fig. 4a lower**), while there is a collective coherence oscillation state of ions confined in the filter. As indicated by our previous results (see **Figs. 2,3**), all the oscillation frequencies of BS-1, BS-2 and filter-confined ion coherence oscillation states are in the range of 39 ~ 41 THz, which leads to that the levels in these states match each other, enabling the K^+ ion tunneling from the KcsA outside to filter resonantly through the bound state between the two barriers.

Relationship of the tunneling-like ion dehydration with the high flux of KcsA channel. To study the effect of tunneling-like ion dehydration on the ion transport efficiency, we performed additional simulations with a frequency-fixed electromagnetic (EM) energy modulation, under the forward and reverse transmembrane voltages of 100 mV, respectively. As the previous analyses shown in **Fig. 2b**, MIR 39.4 THz and 40.6 THz are the coherent oscillation frequencies of filter-confined ions, acting as the resonance channels of transferring energy for the tunneling-like dehydration. Thereby, a MIR EM field of 39.4 THz as a typical example was used to simulate the transferred energy from filter-confined ions, with the strength varied from 0.0 V/nm to 0.6 V/nm **[26,29]**. Under the forward voltage, the tunneling-like dehydration occurs when an ion passes through the hydrophilic gate to Cavity-2 (i.e., Proc-I) and moves from Cavity-2 to filter (i.e., Proc-II), respectively. To describe the dehydration in the processes, we applied the probability (P) of an ion passing through the hydrophilic gate, and the dehydration time (Δt) of an ion moving from Cavity-2 to the site S2, respectively (**Fig. 4b inset**). Under the reverse voltage, an ion achieved complete dehydration as it moved from the sites S03 to S3 (**Supplementary Fig. 2**). The probability P and required time Δt of this process were applied for the dehydration. Based on the P and Δt, we can introduce a parameter (γ) with an identical formula $\gamma = P/\Delta t$ for the dehydration efficiencies under forward and reverse voltages, respectively.

By the parameters above, we analyzed the relationship of tunneling-like ion dehydration with the high flux of KcsA channel. As shown in **Fig. 4b**, when the EM energy strength increased from 0.0 $V\cdot nm^{-1}$ to 0.6 $V\cdot nm^{-1}$, under the forward voltage, the probability P increased from 0.17 ± 0.01 to 0.50 ± 0.02, and the time Δt decreased from 8.14 ± 0.90 ns to 3.91 ± 0.08 ns. The 39.4-THz resonant energy thus can promote both the ion capability of passing through the hydrophilic gate and the ion motion in Cavity-2 to the filter. Under the reverse voltage, the P and Δt kept on plateaus of ~10^{-3} and 339.9 ± 97.4 ns, respectively, denoting no effect of the resonant energy on the process of a hydrated ion moving from the channel exit to filter (i.e., conventional diffusion of hydrated ions). The forward

and reverse dehydration efficiencies γ exponentially increased from 0.022 ± 0.003 ns^{-1} to 0.129 ± 0.006 ns^{-1} and kept on a plateau of 7.8 ± 8.2 10^{-6} ns^{-1}, respectively. The forward and reverse conductance of channel exponentially increased from 4.8 ± 0.5 $e \cdot s^{-1} \cdot V^{-1}$ to 12.0 ± 0.6 $e \cdot s^{-1} \cdot V^{-1}$ and only slightly shifted from plateaus of 6.6 ± 4.1 10^{-4} $e \cdot s^{-1} \cdot V^{-1}$ to 40.0 ± 7.3 10^{-4} $e \cdot s^{-1} \cdot V^{-1}$, respectively. Namely, the dehydration efficiency and conductance followed almost same laws under forward and reverse voltages, respectively, suggesting that the dehydration determines the transport. In the case of EM energy strength at 0.0 $V \cdot nm^{-1}$, i.e., no external EM energy, there is still much large differences in the ion dehydration efficiency and then conductance between the forward and reverse motions, which can be attributed to both the 39.4-THz and 40.6-THz energy resonantly transferred from the filter-confined coherently-oscillating ions. Therefore, the resonant energy transfer within the channel can efficiently promote the tunneling-like ion motion under a forward voltage, but cannot affect the conventional ion diffusion under a reverse voltage, causing the forward rapid dehydration and then the forward high flux of channel.

Note that even if no transmembrane voltage, the resonant energy transfer still occurs when a hydrated ion moves from the channel entrance to filter (not from the exit to filter), causing a 70:1 difference between forward and reverse dehydration, i.e., it is an intrinsic asymmetry of KcsA channel (**Fig. 4c**). In the view of the channel as a body, this dynamics asymmetry leads to a result that the forward flow of hydrated ions through the channel has an intrinsic advantage much greater than the reverse one, providing a basis for the high flux of channel, i.e., relatively the reverse flow is seriously limited.

Finally, it is worth noting that the ultralow energy-consumption rapid ion dehydration and transport highly depend on the ordered structure of ions confined in the channel. Additional electrical and mechanical stimulation thus will cause a structural change in the channel and a disorder in the channel-confined ions, leading to a dramatic decay in the efficiency of channel ion dehydration and

transport. As an inference of our hypothesis, this phenomenon has been observed experimentally, i.e., an electromechanical coupling causes a structure change and consequent inactivation of the potassium channels **[30,31]**.

In summary, by the MD simulations on the KcsA channel system, we demonstrate that a K^+ ion can transfer from the hydration water outside the channel to the water bound in the channel without its hydration water accompanying, i.e., a tunneling-like motion, which provides a basis for the ultralow energy-consumption ion dehydration. During the process, water in the channel remains unchanged. As a hydrated K^+ ion moves from KcsA Cavity-1 to Cavity-2, there occurs a resonant energy transfer to the ion from the filter-confined coherently oscillating ions, causing a tunneling-like motion of the ion from Cavity-1 water to Cavity-2 water with no hydration shell accompanying and no influence on the Cavity-2 water. As the hydrated K^+ ion further moves from Cavity-2 to filter, the ion adjusts its hydration water structure to coherence-resonantly couples with the filter-confined ions, leading to another tunneling-like ion motion to reach complete dehydration. Such two processes cause directionally rapid ion dehydration, which provides a basis for the high flux of KcsA channel. These findings improve our understanding of the physics under the ultralow energy consumption and high flux of ion transport in life systems, potentially promoting the developments in treatment strategies for ion channel-associated diseases and health problems, and in design of bio-inspired materials and devices with ultralow energy consumption.

Methods

Model preparation. We generated an open-state model of the KcsA channel employing the methodology outlined by Koper et al **[23]**. Specifically, A high-resolution protein (PDB code: 1K4C) was applied for the ion-selective filter and a low-resolution protein (PDB code: 3F5W) in open state for the other parts **[32, 33]** (Supplementary Fig. 1). This approach was necessitated by the dearth of

high-resolution (≤ 2 Å) structures depicting the open state of K^+ ion-selective channel protein KcsA, despite the repository containing more than 100 crystallographic entries. The whole protein channel conformation was sufficiently optimized. The advanced Propka tool **[34]** was used to predict the protein protonation state under a pH value of 7.0. Modifications to the protonation state of 71GLU were carried out based on the Bernèche's method **[35]**. To generate the membrane system, the semi-automated processing tool CHARMM-GUI was used with the POPC lipid model. The KcsA protein was embedded in a lipid bilayer consisting of 216 POPC molecules. To enhance the probability of ion transport, the system was placed in a 9 × 9 × 20 nm^3 water box with a concentration of K^+ and Cl^- ions at 0.4 M, consisting of 33,696 water, 218 K^+, and 218 Cl^-.

Simulation setting. All molecular dynamics simulations were performed in the package GROMACS-2019, with the FF14SB and Slipids force fields used for the protein and lipid components, respectively. The water molecules were simulated by the TIP3P model, and the ions by the model of Lee et al **[36]**. Hydrogen bonds were constrained using the linear constraint solver (LINCS) with a time step of 2 fs, and the Verlet scheme was applied to update the neighbor list. Long-range electrostatic interactions were calculated using the particle mesh Ewald (PME) method, with a cutoff of 1.2 nm for electrostatic and van der Waals interactions. The simulation system was maintained at a temperature of 310 K and standard atmospheric pressure, with temperature coupling by the V-rescale thermostat and semi-isotropic Berendsen thermostat for NVT and NPT simulations, respectively.

Firstly, the single bilayer membrane system generated by CHARMM-GUI was minimized for 100 ps, with the protein and lipids allowed to move freely. Then, all heavy atoms except for those in the ion-selective filter (TTVGYG) were restrained with a force constant of 1000 kJ/mol/nm^2 and the system was equilibrated for 20 ns. After the single bilayer membrane system reached equilibrium, the system was duplicated along the z-axis to generate a composite bilayer membrane protein

system, and all heavy atoms in the protein and lipid components except those of filter were restrained with a force constant of 1000 kJ/mol/nm^2 for 20 ns of energy minimization and equilibration. Finally, the simulation protocol of computational electrophysiology in GROMACS (COMPEL) was initiated for 1 μs of production simulation under a fixed charge imbalance Δq = 4 e across the membrane in a fully equilibrated system **[37]**. The charge imbalance Δq leaded to an ion concentration gradient ΔC of 14.6 mM and a resultant transmembrane voltage V. The gmx potential tool was used to calculate V with the relative dielectric constant (ε_r) set as 4 **[38, 39]**. Each of statistics was performed over three 1-μs simulation samples.

References

1. Zhang, X., Song, B. & Jiang, L. From dynamic superwettability to ionic/molecular superfluidity. *Acc. Chem. Res.* **55**, 1195–1204 (2022).
2. Zhang, H., et al. Ultrafast selective transport of alkali metal ions in metal organic frameworks with subnanometer pores. *Sci. Adv.* **4**, eaaq0066 (2018).
3. Li, X., et al. Fast and selective fluoride ion conduction in sub-1-nanometer metal-organic framework channels. *Nat. Commun.* **10**, 2490 (2019).
4. Song, J., Yu, H., Ham, M. & Kim, I. S. Tunable ion sieving of graphene membranes through the control of nitrogen-bonding configuration. *Nano Lett.* **18**, 5506–5513 (2018).
5. Robin, P., Kavokine, N. & Bocquet, L. Modeling of emergent memory and voltage spiking in ionic transport through angstrom-scale slits. *Science* **373**, 687–691 (2021).
6. Xue, Y., et al. Atomic-scale ion transistor with ultrahigh diffusivity. *Science* **372**, 501–503 (2021).
7. Ye, T., et al. Artificial sodium-selective ionic device based on crown-ether crystals with subnanometer pores. *Nat. Commun.* **12**, 5231 (2021).
8. Wei, D., Yang, F., Jiang, Z. & Wang, Z. Flexible iontronics based on 2D nanofluidic material. *Nat. Commun.* **13**, 4965 (2022).
9. Zhang, H., Li, X., Hou, J., Jiang, L. & Wang, H. Angstrom-scale ion channels towards single-ion selectivity. *Chem. Soc. Rev.* **51**, 2224–2254 (2022).
10. Xin, W., et al. Biomimetic KcsA channels with ultra-selective K^+ transport for monovalent ion sieving. *Nat. Commun.* **13**, 1701 (2022).

11. Han, H., et al. Li iontronics in single-crystalline *T*-Nb_2O_5 thin films with vertical ionic transport channels. *Nat. Mater.* **22**, 1128–1135 (2023).
12. Lu, J., et al. An artificial sodium-selective subnanochannel. *Sci. Adv.* **9**, eabq1369 (2023).
13. Chen, W., et al. Cascade-heterogated biphasic gel iontronics for electronic-to-multi-ionic signal transmission. *Science* **382**, 559–565 (2023).
14. Xing, Y., et al. Integrated opposite charge grafting induced ionic-junction fiber. *Nat. Commun.* **14**, 2355 (2023).
15. Zuo, P., et al. Near-frictionless ion transport within triazine framework membranes. *Nature* **617**, 299–305 (2023).
16. Chen, J., Huang, J. & Hu, Y. An optoionic hydrogel with UV-regulated ion conductivity for reprogrammable iontronics: Logic processing and image sensing. *Sci. Adv.* **10**, eadn0439 (2024).
17. Gellrich, C., et al. A precursor-derived ultramicroporous carbon for printing iontronic logic gates and super-varactors. *Adv. Mater.* **36**, 2401336 (2024).
18. Gu, C., et al. In vivo dynamic tracking of cerebral chloride regulation using molecularly tailored liquid/liquid interfacial ultramicro iontronics. *Sci. Adv.* **10**, eadr7218 (2024).
19. Huang, Y., et al. Scalable integration of photoresponsive highly aligned nanochannels for self-powered ionic devices. *Sci. Adv.* **10**, eads5591 (2024).
20. Li, J., et al. An ultrasensitive multimodal intracranial pressure biotelemetric system enabled by exceptional point and iontronics. *Nat. Commun.* **15**, 9557 (2024).
21. Li, X., Li, Y. & Chen, L. Cascade heterointerface-gated iontronics. *Matter* **7**, 299–301 (2024).
22. MacKinnon, R. Potassium channels and the atomic basis of selective ion conduction. *Angew. Chem. Int. Ed.* **43**, 4265–4277 (2004).
23. Köpfer, D. A., et al. Ion permeation in K^+ channels occurs by direct Coulomb knock-on. *Science* **346**, 352-355 (2014).
24. Kratochvil, H. T., et al. Instantaneous ion configurations in the K^+ ion channel selectivity filter revealed by 2D IR spectroscopy. *Science* **353**, 1040–1044 (2016).
25. Kopec, W., et al. Direct knock-on of desolvated ions governs strict ion selectivity in K^+ channels. *Nat. Chem.* **10**, 813–820 (2018).
26. Wang, Y., et al. A physical derivation of high-flux ion transport in biological channel via quantum ion coherence. *Nat. Commun.* **15**, 7189 (2024).
27. Hille, B. *Ion Channels of Excitable Membranes* (Sunderland, Mass., Sinauer Associates Inc., 2001).
28. Planck, M. Zur theorie des gesetzes der energieverteilung im normalspectrum. *Verh. Dtsch. Phys. Ges.* **2**, 237–245 (1900).
29. Zhu, Z., Chang, C., Shu, Y. & Song, B. Transition to a superpermeation phase of confined water induced by a terahertz electromagnetic wave. *J. Phys. Chem. Lett.* **11**, 256–262 (2019).
30. Fernández-Mariño, A. I., Tan, X.-F., Bae, C., Huffer, K., Jiang, J. & Swartz, K. J. Inactivation of the Kv2.1 channel through electromechanical coupling. *Nature* **622**, 410–417 (2010).
31. Tan, X.-F., Fernández-Mariño, A. I., Li, Y., Chang, T.-H. & Swartz, K. J. Structural basis of fast N-type inactivation in K_v channels. *Nature* **645**, 1081–1089 (2025).

410 32. Zhou, Y., Morais-Cabral, J. H., Kaufman, A. & MacKinnon, R. Chemistry of ion coordination and hydration revealed
411 by a K^+ channel-Fab complex at 2.0 Å resolution. *Nature* **414**, 43–48 (2001).
412 33. Cuello, L. G., Jogini, V., Cortes, D. M. & Perozo, E. Structural mechanism of C-type inactivation in K^+ channels.
413 *Nature* **466**, 203–208 (2010).
414 34. Søndergaard C. R., Olsson M. H. M., Rostkowski M. & Jensen J. H. Improved treatment of ligands and coupling
415 effects in empirical calculation and rationalization of pK_a values. *J. Chem. Theory Comput.* **7**, 2284–2295 (2011).
416 35. Berneche S. & Roux B. The ionization state and the conformation of Glu-71 in the KcsA K^+ channel. *Biophys. J.* **82**,
417 772–780 (2002).
418 36. Lee K. I., S., et al. Web interface for Brownian dynamics simulation of ion transport and its applications to beta-
419 barrel pores. *J. Comput. Chem*. **33**, 331–339 (2012).
420 37. Kutzner C., Grubmüller H., de Groot B. L. & Zachariae U. Computational electrophysiology: The molecular
421 dynamics of ion channel permeation and selectivity in atomistic detail. *Biophys. J.* **101**, 809–817 (2011).
422 38. Schutz C. N. & Warshel A. What are the dielectric "constants" of proteins and how to validate electrostatic models?
423 *Proteins* **44**, 400-417 (2001).
424 39. Li L., Li C., Zhang Z. & Alexov E. On the Dielectric "Constant" of Proteins: Smooth Dielectric Function for
425 Macromolecular Modeling and Its Implementation in DelPhi. *J. Chem. Theory Comput.* **9**, 1865-2150 (2013).
426

427 ## Acknowledgements

428 This work was supported by the National Key R&D Program of China (2021YFA1200404, B.S.), the National Natural
429 Science Foundation of China (T22410002, B.S.; T2394532, B.S.).

430 ## Author contributions

431 B.S. and L.J. conceived the study. B.S. designed the MD simulations, and Y.W. performed the MD simulations. All authors
432 analyzed the results. B.S., L.J. and Y.W. wrote the manuscript.

433 ## Competing interests

434 The authors declare no competing interests.

435

Figures and Legends

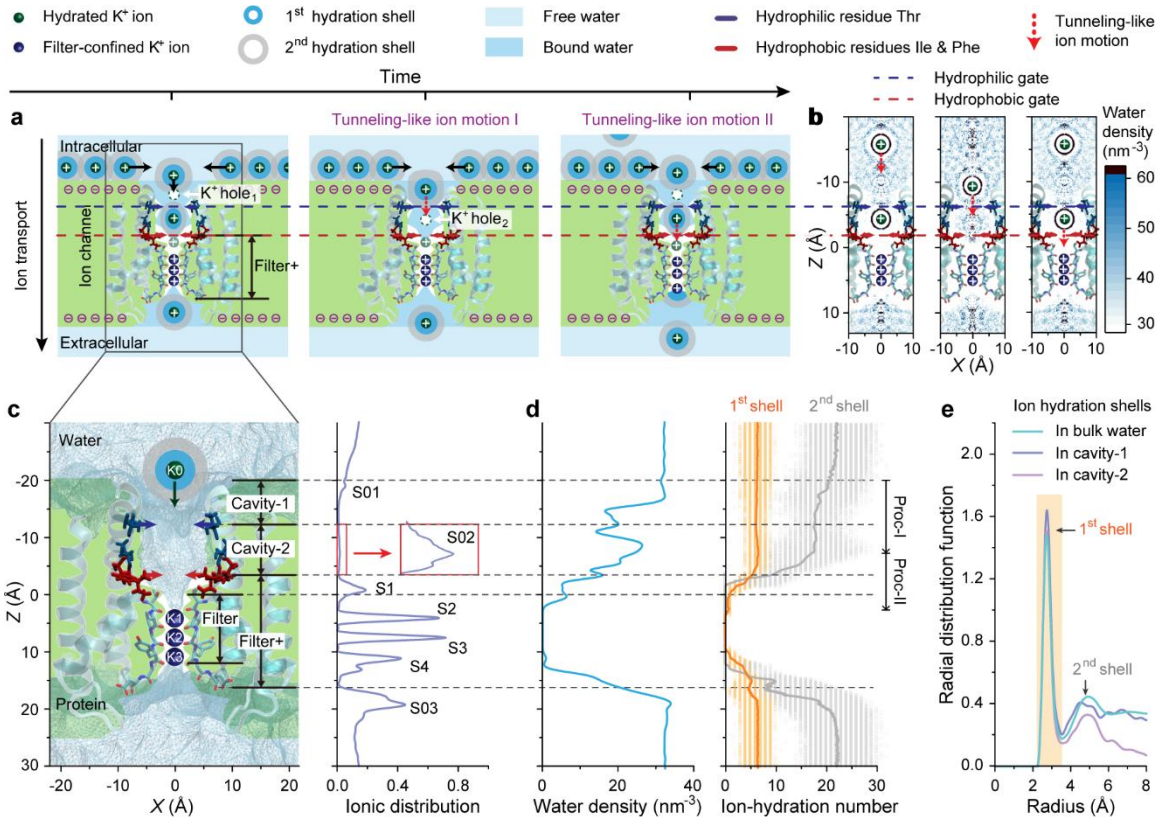

Fig. 1 | Hypothesis of tunneling-like K^+ ion dehydration in a KcsA channel together with the molecular dynamics simulation system and preliminary analyses. a) Hypothesis of tunneling-like K^+ ion dehydration in a KcsA channel. Left: A hydrated ion (K0') outside of the channel moves to the channel Cavity-1. Middle and right: An ion (K0) conducts a tunneling-like motion (dotted red arrow) from the Cavity-1 to Cavity-2 water (middle) and from the Cavity-2 water to Filter+ (right). The K0 ion passes through the hydrophilic (dark blue) and hydrophobic (dark red) gates of channel without its hydration shell accompanying, distinguished from the conventional diffusion of a hydrated ion. The water in Cavity-2 remains unchanged in the processes, i.e., its changes caused by the ion is ignorable. **b-e)** KcsA channel system and water analyses of ion dehydration. **c)** Simulation system under a transmembrane voltage (*V*) of 100 mV (left) and the ion-occupation sites of channel (right). The light blue network indicates the spatial distribution of water, while the white and green parts denote the areas of protein pore and protein, respectively. **d)** Distributions of water density and ion hydration number. The orange and gray curves mean the ion 1st- and 2nd-shell water, respectively.

Proc-I and Proc-II denote the dehydration-related processes of an ion moving from Cavity-1 to Cavity-2 and from Cavity-2 to the filter, respectively. **e)** Radial distributions of ion shell water in Cavity-1 (light blue) and Cavity-2 (violet).

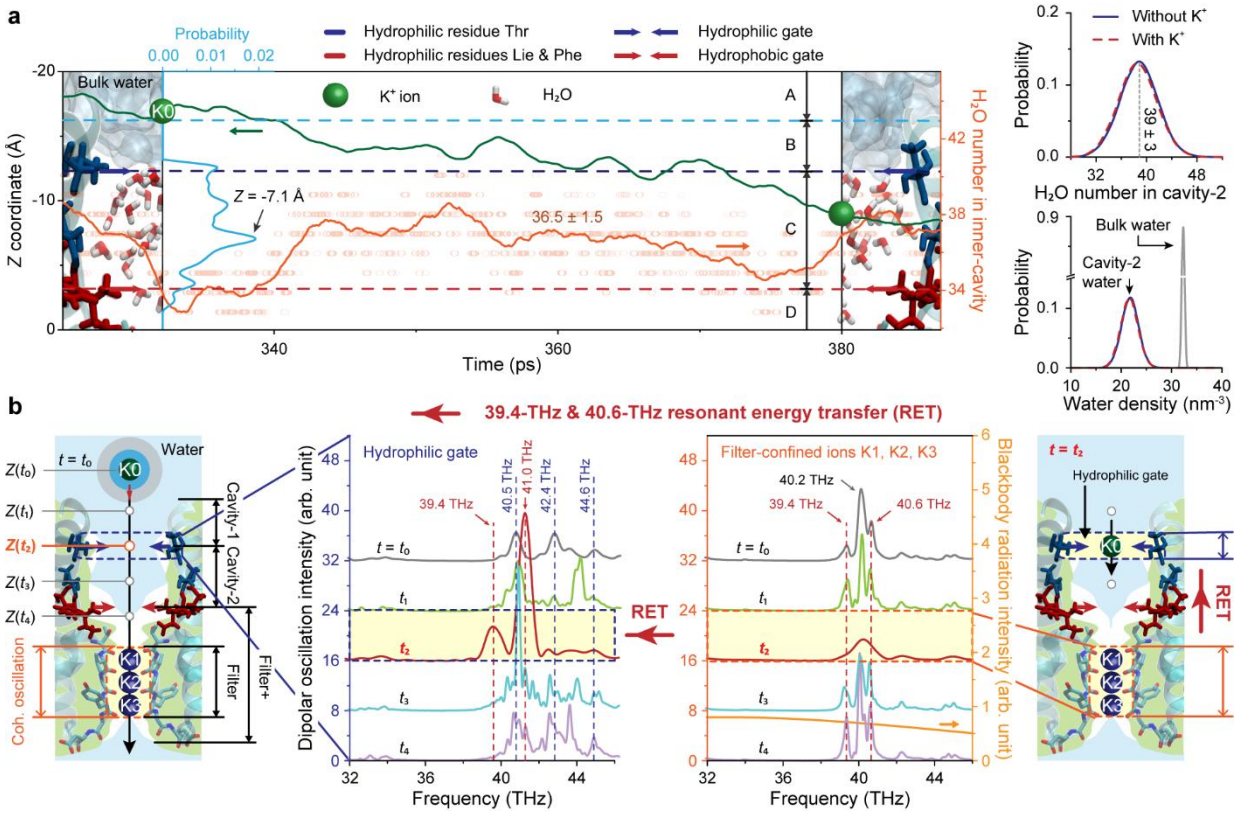

Fig. 2 | Resonant energy transfer-driven tunneling-like dehydration as a K^+ ion moves from KcsA Cavity-1 to Cavity-2. a) Replacement of K^+ ion hydration shell by a new one when the ion passes through the hydrophilic gate, i.e., tunneling-like ion dehydration. Left: Typical trajectories of the K^+ ion coordinate (green) and Cavity-2 H_2O number (tangerine, circles for the instantaneous values). The light blue curve stands for the H_2O distribution in Cavity-2. Right: Distributions of Cavity-2 H_2O number (right upper) and water density (right lower) in absence (blue) and presence (red) of K^+ ions over all the simulations. The gray curve indicates the bulk water. **b)** Resonant energy transfer (RET) from the filter-confined K^+ ions (K1, K2, K3) to hydrated ion (K0) as the K0 passes through the hydrophilic gate. Left: Schematic representation of K0 moving from the outside of channel toward the filter. The label $Z(t_i)$ means the Z coordinate of K0 at the time t_i (i = 0, 1, 2, 3, 4). Middle: Dynamics spectra of the hydrophilic gate (middle left) and filter-confined K^+ ions (middle right). The gray, green, red, blue and violet curves denote the spectra at the time $t = t_0$, t_1, t_2, t_3 and t_4, respectively. Right: Schematic representation of RET from the filter-confined ions to ion-coupled hydrophilic gate as the K0 is at the hydrophilic gate ($t = t_2$).

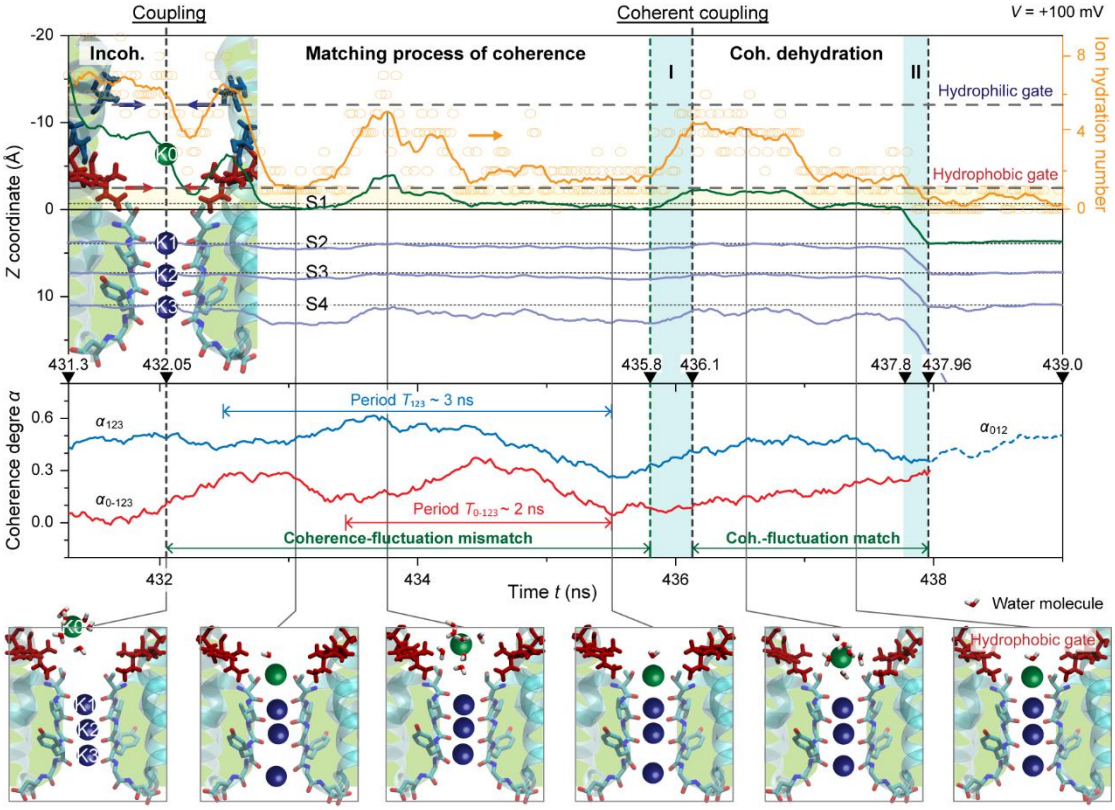

Fig. 3 | Coherent resonance-caused tunneling-like dehydration as a K^+ ion moves from KcsA Cavity-2 to filter. The green and blue spheres indicate the K^+ ions initially in the Cavity-2 (K0) and filter (K1, K2, K3), respectively. Top: *Z*-coordinate trajectories of K^+ ions (green for K0 and gray blue for K1, K2, K3) and K0 1st-shell H_2O number (orange, circles for the instantaneous values). Middle Trajectories of the ion coherence degree *α*. The red and light blue curves indicate the coherence degree of K0 with three filter-confined ions (K1, K2, K3) and that of the three filter-confined ions (blue solid: K1, K2, K3 for $t < 437.96$ ns, blue dashed: K0, K1, K2 for $t > 437.96$ ns), respectively. Bottom: Typical conformations of the hydrated K0 ion in the process.

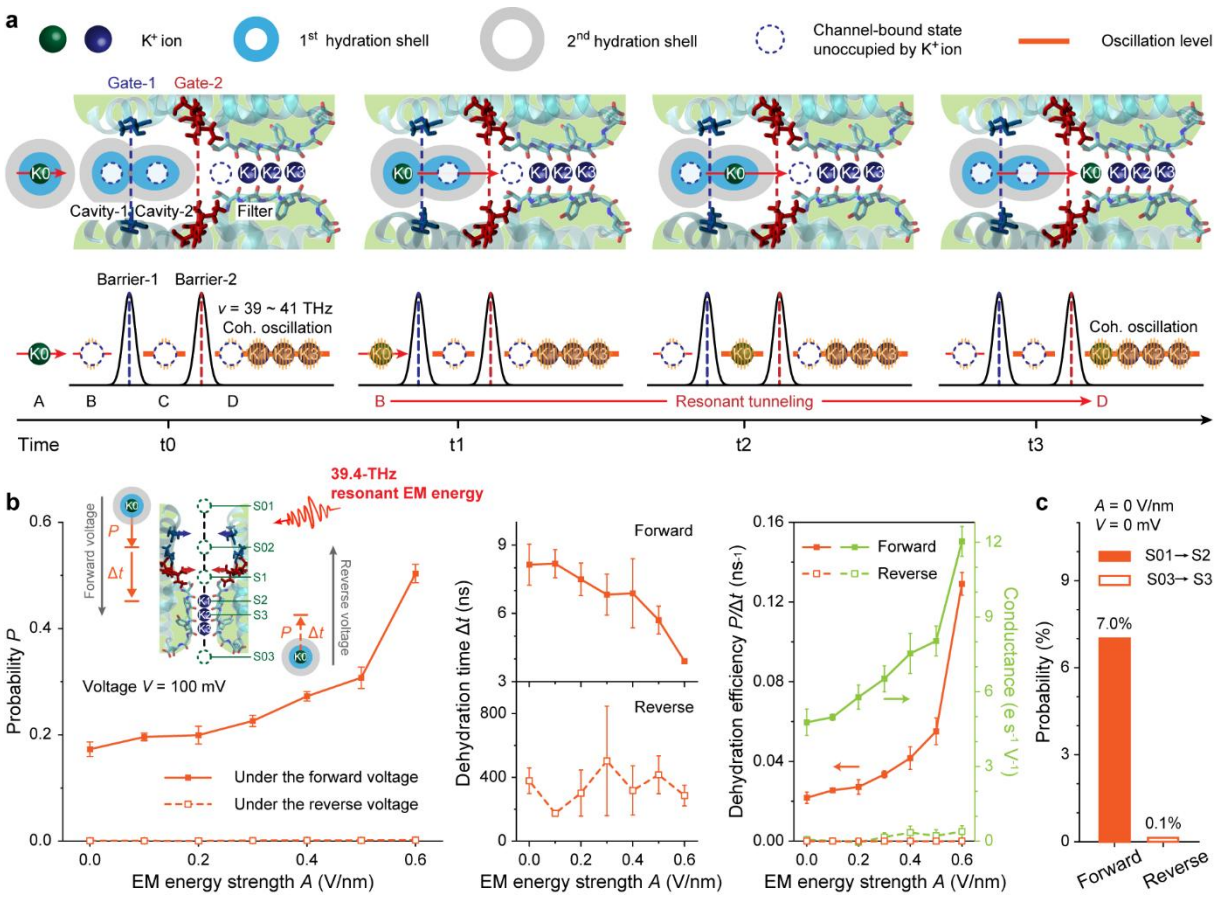

Fig. 4 | Resonant tunneling of ion from the KcsA outside to filter and its relation with the high flux of KcsA channel. a) Schematic representation of the resonant ion tunneling. The green and blue spheres indicate the K^+ ions initially in the outside (K0) and filter (K1, K2, K3), respectively. Upper: Locations of K^+ ions as the K0 moves from the KcsA outside to filter. The dark blue and dark red stands for the hydrophilic and hydrophobic gates, i.e., Gate-1 and Gate-2, respectively. Lower: Level structures for the K0 ion to perform the resonant tunneling. **b)** Resonant energy effect on the dehydration and transport efficiencies of channel under the forward and reverse transmembrane voltages with an identical strength V = 100 mV. The resonant electro-magnetic (EM) energy, with a frequency (39.4 THz) identical to that of filter-confined ion coherence oscillation, is added to the channel (inset). Left: Probabilities (P) of the ion moving from the sites S01 to S02 (i.e., tunneling-like ion motion) under the forward voltage and from the sites S03 to S3 (i.e., conventional diffusion of hydrated ions) under the reverse, respectively. Middle: Time (Δt) required for the complete

dehydration as the ion moves from the sites S02 to S2 (tunneling-like motion) under the forward voltage and from the sites S03 to S3 (conventional diffusion) under the reverse one, respectively. Right: Dehydration efficiency (tangerine) and conductance (green) under the forward and reverse voltages. **c)** Effect of the resonant energy transfer of filter-confined ions on the forward and reverse ion motion in absence of the external EM energy and transmembrane voltage.

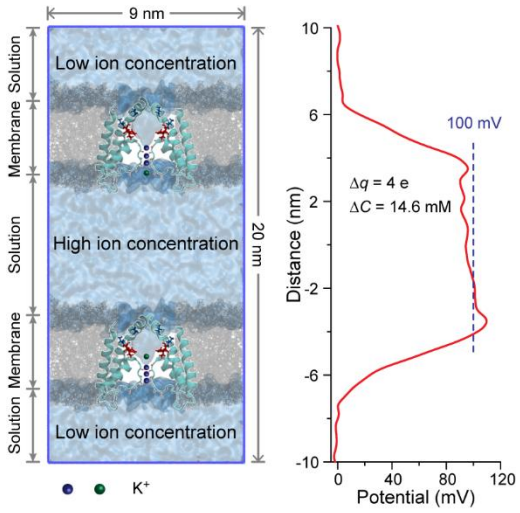

Supplementary Fig. 1 | The whole simulation system and its potential change caused by transmembrane ion concentration difference. The labels Δ*q* and Δ*C* mean the charge imbalance and ion concentration difference, respectively.

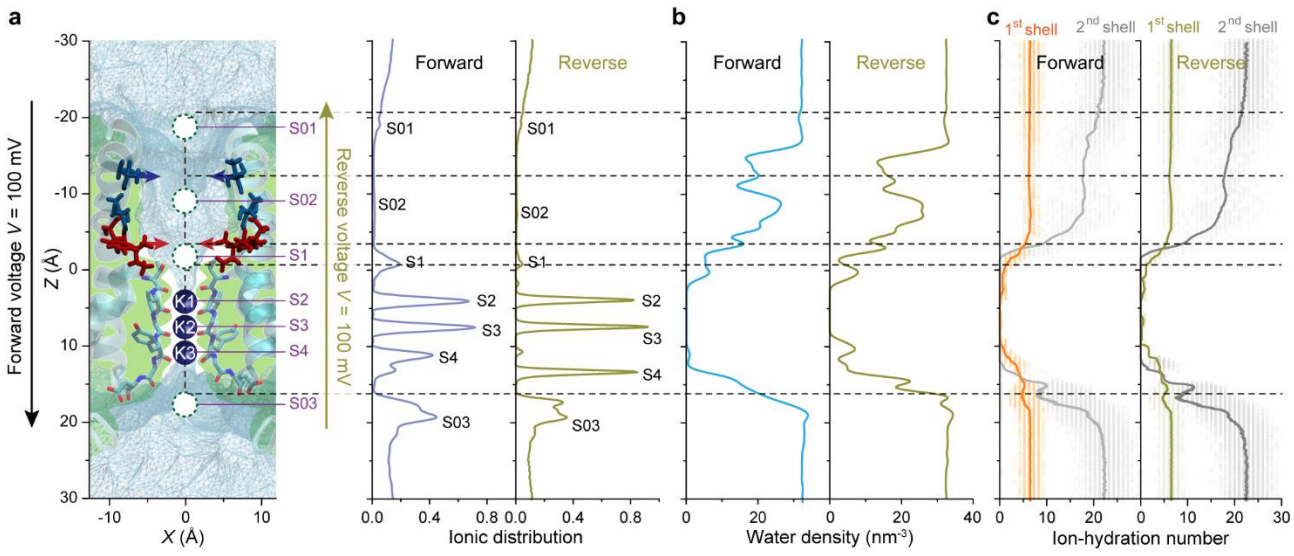

Supplementary Fig. 2 | Distribution analyses of ions and water molecules in the KcsA channel under forward and reverse voltages. a) Ion-occupation sites in the channel under forward (middle) and reverse (right) transmembrane voltages (*V*) of 100 mV. **b)** Distributions of water densities under the forward (left) and reverse (right) voltages. **c)** Ion hydration numbers of the 1st- and 2nd-shell water under the forward (left) and reverse (right) voltages.